Thermo-Physical Optimisation of Specialised Concrete Pavement Materials for Surface Heat Energy Collection and Shallow Heat Storage Applications

Pejman Keikhaei Dehdezi*, Matthew R Hall, Andrew Dawson

Pejman Keikhaei Dehdezi*

Nottingham Transport Engineering Centre, Division of Infrastructure and Geomatics, Faculty of Engineering, University of Nottingham, University Park, NG7 2RD, UK Tel: +44 (0) 115 823 2423, Fax: +44 (0) 115 951 3159, E-mail: evxpk3@nottingham.ac.uk

Matthew Hall

Nottingham Centre for Geomechanics, Division of Materials, Mechanics and Structures, Faculty of Engineering, University of Nottingham, University Park, NG7 2RD, UK Tel: +44 (0) 115 846 7873, Fax: +44 (0) 115 951 3159, E-mail: matthew.hall@nottingham.ac.uk

Andrew Dawson

Nottingham Transport Engineering Centre, Division of Infrastructure and Geomatics, Faculty of Engineering, University of Nottingham, University Park, NG7 2RD, UK Tel: +44 (0) 115 951 3902, E-mail: E-mail: andrew.dawson@nottingham.ac.uk

* Correspondence author

Word Count: 4101 text, 3 Tables and 10 Figures (Total= 7351)

Submission date: 24/Feb/2011

ABSTRACT

There is great potential to use pavement structures to collect and/or store solar energy for the heating and cooling of adjacent buildings, e.g. airport terminals, shopping malls, etc. Therefore, pavement materials comprising both conventional and unconventional concrete mixtures with a wide range of densities, thermal conductivities, specific heat capacities, and thermal diffusivities were investigated. Their thermo-physical properties were then used as inputs to a one dimensional transient heat transport model in order to evaluate the temperature changes at the various depths at which heat might be abstracted or stored. The results indicated that a high diffusivity pavement, e.g. incorporating high conductive aggregates and/or metallic fibres, can significantly enhance heat transfer as well as reduction of thermal stresses across the concrete slab. On the other hand a low diffusivity concrete can induce a more stable temperature at shallower depth enabling easier heat storage in the pavement as well as helping to reduce the risk of damage due to freeze-thaw cycling in cold regions.

INTRODUCTION

Many buildings that have a high heating and/or cooling load are built adjacent to roads, aircraft stands, car parks, etc. (e.g. airport terminals, shopping malls, factories, warehouses, and retail outlets). Therefore, there is great potential to collect and/or store solar energy using the large adjacent pavement surface areas which are already required for operational reasons. Such pavement structures, equipped with fluid-filled pipes (known as 'loops'), are here termed 'Solar Pavements'.

Solar pavements could be used (Figure 1) either by installing loops close to the pavement surface in order to collect the solar energy (Pavement Heat Collectors - PHC), or by installing loops at shallow depths in order to use the pavement as a heat source during winter and as a heat sink during summer (Pavement-Source Heat Stores - PSHS). The two systems might be combined or linked together as a hybrid system by which the solar heat collected by the pavement surface in the summer is transferred and stored in shallow insulated ground heat stores for subsequent re-use (*1*). In all applications, the transmitted heat to the loops could also be used, either directly or in conjunction with a heat pump, for different purposes such as de-icing of the roads in winter, to reduce the urban heat island effect, to reduce asphaltic pavement rutting, to heat or cool adjacent buildings, to supply hot water, or to convert the energy to a transmittable form (*1, 2*). If such a system were to be installed at the time of pavement construction, it might incur only a marginal cost as the cost of the pavement construction would probably be already funded from a separate budget (i.e. a budget for transportation rather than energy purposes).

Figure 1 goes here

The thermo-physical properties of pavement materials along with an effective loop component design (i.e. depth of pipe burial, type and length of pipes, type of fluid, etc) are key parameters to design solar pavements. Previous studies have shown that thermo-physical properties of pavement materials have a significant effect on temperature distribution within the pavement (*3,4,5*).

OBJECTIVE

The objective of this paper is to study the thermo-physical properties of concrete pavement materials and determine their effects on the performance of PHC and PSHS and other implications to help pavement design. Thermo-physical properties of concrete pavements with acceptable mechanical qualities for different structural applications (e.g. roads, aircraft stands, car parks) were used in a one-dimensional transient heat transport model which was previously developed and verified by the authors (*5*).

THERMAL, PHYSICAL AND MECHANICAL PROPERTIES OF MODIFIED PAVEMENT MATERIALS

A wide range of heavy-weight, light-weight, and normal aggregates, as well as other additives, were used to produce concrete that might deliver beneficial thermo-physical properties. Replacement components included limestone, quartzite, natural sand, sintered pulverised fuel ash lightweight aggregate (known as 'Lytag'©), crumb rubber, cooled iron shot (known as 'Ferag'©), air cooled copper slag, Incinerator bottom ash, furnace bottom ash, and copper fibre. Pavement Quality Concrete (PQC) and Lean Mix Concrete (LMC) mixes were designed according to airfield concrete pavement design (*6*) The control mix for PQC used is a 10/20 single sized limestone aggregate and 4mm down natural sand in compliance with BS EN 12620 (*7*) as well as high strength Portland cement (CEM I, 52.5 N/mm^2). The control mix for LMC used is an all-in limestone aggregate and CEM I, 52.5 N/mm^2. Particle density and water absorption coefficients of the materials were experimentally determined according to BS EN 1097-6 (*8*). Based on these values, the volumetric replacement method was used in calculating the mixture proportions. All concrete specimens were first air cured for 24h in laboratory conditions, and then for a period of 28 days in water at a temperature of 20 °C ± 2 °C.

Five 100mm cubes were used for the determination of unconfined compressive strength (f_c), according to BS EN 12390-3 (*9*). Apparent Porosity (*AP*) of specimens was assessed using the following expression:

$$AP(\%) = \frac{w_s - w_o}{w_s - w_w} \times 100 \quad (1)$$

w_s is the weight of the specimen at the saturated condition, w_w is the weight of the specimen in water under saturated conditions and w_o is the dry weight of the specimen when dried to constant mass at 105±5˚C for 24 h. The mean values of all measured parameters along with saturated surface dry density (ρ_{ssd}) and dry density (ρ_d) of the concretes are presented in Table 1. The thermal conductivity of the concrete specimens, following immersion in water (λ*) and oven-dried (λ) conditions, were experimentally determined using a computer-controlled P.A. Hilton B480 uni-axial heat flow meter apparatus with downward vertical heat flow, which complies with ISO 8301 (*10*). The concrete slab specimens were placed inside the apparatus between a temperature-controlled hot plate and a water-cooled cold plate connected to a separate chiller device. Under steady state conditions, the thermal conductivity of the specimen is calculated using:

$$\lambda\ (or \lambda^*) = \frac{l_s\left[(k_1 + (k_2.\overline{T})) + ((k_3 + (k_4.T)).HFM) + ((k_5 + (k_6.\overline{T})).HFM^2)\right]}{dT} \quad (2)$$

Where

k_1-k_6 calibration constants of the apparatus determined separately

$\bar{T} = \frac{T_{hot} + T_{cold}}{2}$ average temperature of hot & cold plate

$dT = T_{hot} - T_{cold}$

The values for the calibration constants of the apparatus k_1-k_6 inclusive are determined separately, and the heat flowmeter output (HFM) is measured in mV. Steady state conditions are deemed to occure when the percentage variation in heat flux throughout the sample is≤3%. The sample interval of the heat flow meter is given by the greater of 300 or

$$\rho C_s l_s R \quad (3)$$

Where

ρ	density of the specimen,
C_s	specific heat capacity of the specimen,
l_s	thickness of the specimen,
R	specific thermal resistance of the material

Two slabs with dimensions of 300×300mm, and a thickness of approximately 65mm, were prepared for each mix design and then the mean value of three independent readings was obtained for each slab specimen at oven-dried and water immersed states. For thermal conductivity measurement in wet state, the concrete slabs were removed from the curing tank water at the end of their 28-day curing period and sealed in a vapour-tight envelop to prevent a change in moisture content. The influence of the thin envelop on the thermal conductivity of the slab specimens was found to be negligible when measuring thermal conductivity at a steady state variance of ± 2 - 3%, as prescribed by ISO 8301 (*10*). In the dry state, all the specimens were dried in an oven at 105±5˚C, until the mass changes by less than 0.2 % in 24 h, and then cooled in a desiccator. More details about the test can be found in a previous publication (*5*).

The specific heat capacity of each mix design was calculated as the sum of the heat capacities of the constituent parts weighted by their relative proportions. Therefore, the specific heat capacity of Hardened Cement Paste (HCP) was first measured and then the specific heat capacity of Coarse Aggregates (CA), Fine Aggregates (FA), and Additives (ADD) were added proportionally, it was assumed that air in the samples had a negligible contribution to the heat capacity of the total concrete since it has a density of approximately 1.205 kg/m^3 at ambient temperatures compared to 2300 kg/m^3 for the concrete solids. The specific heat capacity of concrete in both the dry (c_p) and wet (c_p*) states are calculated from equations 4 and 5, respectively.

$$c_p = \frac{1}{w_{TOTAL}} \left[w_{HCP} c_{HCP} + w_{CA} c_{CA} + w_{ADD} c_{ADD} \right] \quad (4)$$

$$c_p^* = c_p + \frac{AP \times \rho_{water}}{w_{water}} \times c_{water} \quad (5)$$

w = mass of each constituent in kg, c = specific heat capacity of each constituents in J/kg K.
A Differential Scanning Calorimeter (TA Instruments Model Q10 DSC) was used to determine the specific heat capacity of the concrete constituents. The mean value of five readings taken across the range -13 ˚C to 57 ˚C is presented for each component in Table 2.
Thermal diffusivity (α) is the coefficient that expresses the rapidity of temperature change when a material is exposed to a fluctuating thermal environment and is calculated as:

$$\alpha = \frac{\lambda}{\rho_d c_p} \quad (6)$$

Thermal effusivity (β), also known as the coefficient of heat storage, is a measure of material's ability to exchange heat with its surroundings and is calculated as follows:

$$\beta = \sqrt{\lambda \rho_d c_p} \quad (7)$$

The wet-state thermal diffusivity (α*) and thermal effusivity (β*) of concretes were also calculated by inserting the wet values in the above equations. The mean values of measured and calculated thermal properties of modified concrete pavements are presented in Table 3.

Table 1 goes here

Table 2 goes here

Table 3 goes here

PREDICTIVE NUMERICAL MODELLING TOOL

A one-dimensional transient heat transport model (*5*) is used in this paper to predict the response of pavements constructed using some of the novel materials listed in Table 2 and 3. The model was previously developed to predict pavement temperature profile evolution at various different depths in response to the climatic variables period. Keikha et al (*5*) validated the model using data provided by the Seasonal Monitoring Program (SMP) database of the Long-Term Pavement Performance program (LTPP) project (*12*). The model is accurate to within 2˚C variation (*5*) and was found to give results at least as good as other similar available models (*3*,*4*).

FACTORS AFFECTING CONCRETE THERMAL PROPERTIES

It is evident from the data presented in Table 3 that the degree of saturation correlates to a significant increase in the thermal conductivity for each concrete material that was tested. This can be attributed to changes in air voids filled with water, whose thermal conductivity is superior to that of air. However, it was also observed that the thermal conductivity of the concrete was directly and positively related to that of the aggregate. Quartzite aggregate, for example, has a conductivity between 5.5 - 7.5 W/m K (*15*) and produced concrete with a conductivity of 2.8 W/m K in this study, whereas limestone which has a conductivity range of 1.5 - 3.0 (*15*) produced concrete with a conductivity of 1.4 W/m K, this is also the case for synthetic alternative aggregates such as Lytag and crumb rubber. There are probably other reasons for change in thermal conductivity which maybe as, or more significant, than changes in the thermal conductivity of the aggregate. For example, crumb rubber modified concrete is known to have problematic interfacial transition zones (*16*) which are likely to augment reductions in thermal conductivity. Figure 2 shows an inverse relationship between the apparent porosity and both the dry and saturated thermal conductivity for Lytag- and crumb rubber-modified concretes. It is assumed that this can occur as a result of enhanced inter-particle contact when the void ratio is minimised.

Figure 2 goes here

Interestingly, the addition of cooled iron shot particles had minimal effect on the thermal conductivity of PQC. The thermal conductivity of cast iron is known to be approximately 45 W/m K at 25 deg C (*17*). However, when loose cooled iron shot particles were tested using a Setaram TCi modified transient plane source device, the thermal conductivity was determined to be only 1.4 W/m K in the dry state. This reduction must be a reflection of the very limited inter-particle contact. Figure 3a, is a cross-sectional image through the concrete containing cooled iron shot particles produced using a Venlo H 225/350 X-Ray Computer Tomographic (XRCT) scanner at 83 micron resolution and 340 kV accelerating voltage. It shows that even though there are some clusters of iron shot which might

deliver a conductivity of 1.4 W/m K, these clusters are not well interconnected further reducing their opportunity to convey heat energy effectively through concrete. Comparison of λ values in Table 3 for "with" and "without" iron shot particles (see 24 and 10 respectively) will illustrate this.

On the other hand, the results of experiments carried out by Cook and Uher (*11*) proved that the addition of steel and copper fibre in concrete can significantly improve the thermal conductivity of the concrete. Figure 3b shows that the addition of metallic fibre in concrete can develop many continuous highly conductive paths that as expected increase the thermal conductivity of the concrete. This effect can be seen in Table 3 comparing values of λ for mixes 4-9 which are those with increasing copper fibre content.

Figure 3 goes here

MATERIALS DESIGN OPTIMISATION FOR PHC APPLICATIONS

The efficiency of a PHC system in transporting large quantities of heat from the pavement surface to the embedded pipe network depends on several key factors:

1) The ability of the pavement to absorb heat at/near the surface-air interface
2) The ability to conduct heat between the pavement surface and the pavement sub-surface
3) The depth of the embedded pipe network
4) The materials, geometry, spacing, and dimensions of the pipes
5) The type of working fluid within the pipes
6) The initial temperature and flow rate of the working fluid
7) The pavement material-pipe interface, i.e. the ratio of specific surface area to area in contact.

Factors 1 to 3 are the focus of this study as they are related to the design of civil engineering materials issues and have, to date, received little attention. Factors 4 to 7 are mechanical systems engineering issues relating to the operation of the system and the working fluid and, whilst being the focus of much previous research, significant potential exists for collaboration combining the work presented here with that previous thermo-fluid research work so as to deliver a comprehensive study simultaneously considering all of the factors mentioned.

The quantity of heat energy absorbed by the pavement is directly proportional to the pavement surface absorptivity which is mainly related to the pavement surface colour. Yavuzturk et al (*3*) reported that the maximum temperature change at the pavement surface is as high as 10˚C when the absorptivity is altered between 0.5 and 0.99. This work is focused on concrete pavement materials which would typically have a solar absorptivity of about 0.65, but with the additional of a high-absorptivity coloured surface coating can achieve in excess of 0.9 (*3*,*18*). In order to represent optimised heat collection conditions, the thermal model used a high value of 0.95 in order to simulate the best performance of PHCs.

Figure 4 shows the cross-section of an existing pavement in Arizona and four other modified sections. The climatic data and pavement sections were extracted from the SMP conducted under the LTPP (*12*) for the state of Arizona, USA. This was chosen as it is a prime location for a PHC installation where solar radiation exceeds 1000 W/m^2 in summer, and so representing a 'best case' performance scenario. The Arizona LTPP pavement climatic data were collected at weather station number 0100, between 01/01/1996 to 31/12/1996.

Figure 4 goes here

Installing the pipe network very close to the surface of the pavement (e.g. <50mm depth) obviously provides higher temperature heat energy for absorption by the working fluid. Ideally, sufficient depth is required in order to avoid 'reflection cracking' under traffic loading, which has a detrimental effect on the lifespan of the pavement, and also to enable future resurfacing without damaging the pipe network. By applying the thermo-physical properties of pavement layers in the thermal model, the mean maximum temperature for each month in Arizona has been plotted at two depths; 40mm and 120mm (see Figure 5). These depths were chosen based on the embedded pipe depths in previous full-scale PHC trials by Ooms Avenhorn Holding (*2*) and the Transport Research Laboratory (*1*), respectively.

Figure 5 shows that by using PHC Design #2 the same temperature can be achieved at a depth of 120mm, as the temperature at 40mm depth in the unmodified reference pavement. The presence of a high thermal diffusivity pavement layer above a depth of 120mm, combined with a high thermal resistance pavement layer below this depth, (i.e. PHC Design #4) can significantly increase the temperature at pipe locations, as shown in Figure 5. Theoretically, this would result in a significant increase in the efficiency of a PHC system. Additionally, there is no significant difference between the temperatures at 40mm and 120mm in PHC Design #4 since the high diffusivity material layer allows heat to penetrate rapidly into the pavement.

Figure 5 goes here

Figure 6 compares the predicted daily temperature fluctuation throughout July for the unmodified reference pavement and PHC Design #4, at a depth of 40mm. The maximum temperature, which occurs just after midday, increases by an average of 6˚C for the optimised PHC design. This can be attributed to the fact that a pavement with higher thermal diffusivity allows the heat gain from the solar radiation at the surface to be transferred into the pavement much more rapidly, whilst the higher thermal resistance of the lower layers reduces heat loss to the sub-soil. Conversely, the minimum surface temperature, which occurs during the night, decreases by about 2˚C for PHC Design #4 since more heat is dissipated from the surface to the ambient environment. In locations with high solar

irradiation ($\geq$1000 W/m^2) the low-grade heat energy absorbed by the working fluid in the embedded pipes can be upgraded by a heat pump and converted to a transmittable form by exploiting binary-type energy conversion systems such as Kalina cycles that are typically used to exploit low-temperature geothermal resources, typically 85˚ C or less (*15*). Higher temperature heat energy (i.e. higher pavement temperature at depths for pipe embedment) obviously increases the efficiency of the heat pump. Nevertheless, water circulating in a pipe network could also be used directly or as a heating system for swimming pools which are usually operated at between 20˚C and 27˚C (*19*).

Figure 6 goes here

One of the advantages of using high thermal diffusivity concrete pavement materials is to reduce the warping stresses that can occur due to temperature differences between the top and bottom of the slab. To illustrate this, Figure 7 compares the temperature distribution within the reference pavement, and PHC Designs #1, #2, and #3 at 4am and 4pm in July. It can be seen that as the concrete thermal diffusivity increases, the temperature gradient range across the slab (120mm thickness) will decrease considerably. Therefore the service life of the pavement can be prolonged due to the reduction of thermal stresses. In addition, the total temperature variations between 4 am and 4 pm reduce as thermal diffusivity increases, which could minimise the likelihood of thermal cracking from expansion and contraction.

Figure 7 goes here

MATERIAL DESIGN OPTIMISATION FOR PSHS APPLICATIONS

Ground Source Heat Pumps (GSHPs) rely on the fact that, at depth, the Earth's crust has a relatively constant temperature; warmer than the air in winter and cooler than the air in summer. A reversible heat pump can transfer heat stored in the Earth into a building during the winter, and transfer heat out of the building during the summer. The efficiency of GSHPs can significantly increase if the temperature variations at the pipe location(s) is minimised, as is the case for vertical GSHPs that have significantly higher efficiency than horizontal GSHPs (*16*). Pavements are already required for essential infrastructure purposes, having a set of structural performance criteria to meet, and so would only need a few thermally-specific elements to be installed in order to act as a thermal heat storage system as is the case with conventional thermal energy utilisation systems. However, the thermal properties of the pavement constituent material have not, previously, been optimised for these purposes. Therefore, PSHSs as an innovative technology might be designed to operate more cost-effectively than conventional GSHPs.

Five different pavement cross- sections with different thermo-physical properties are considered (see Figure 8) and the mean February and July temperature distributions within these pavements have been predicted using the numerical model mentioned earlier in the section "Predictive numerical modelling tool". The pavement cross-sections represent an airport apron since this is a key potential application for this technology. Airport buildings have, typically, high cooling loads and energy demands and are immediately adjacent to large areas of pavement surface. They are also of a similar arrangement throughout the world. The climatic data for this PSHS simulation was collected from the University of Nottingham weather station at Sutton Bonington, Leicestershire, UK (52.58˚N, 1.38˚W), which is close to East Midlands Airport.

Figure 8 goes here

The critical depth (d_{crit}) below the surface at which minimal seasonal temperature fluctuation occurs is defined by the point of convergence between seasonal minima and maxima. From previous research conducted by the authors, this is known to be positively correlated to the thermal diffusivity of pavement materials (*7*). The effect of the pavement's thermal diffusivity on d_{crit} is shown in Figure 9. It can be seen that as the thermal diffusivity decreases d_{crit} will also decrease. This is because the material with higher Volumetric Heat Capacity (VHC), equal to ρc, and lower thermal conductivity will reduce the temperature fluctuation at a lower depth within the pavement.

Figure 9 goes here

Figure 10 shows the temperature fluctuation between 01/01/2007 to 26/12/2007 at a depth of 1.5m. It can be seen that temperature fluctuation at this depth is minimised as the pavement thermal diffusivity decreases (refer to Figure 8 for PSHS design). Less temperature fluctuation will improve the efficiency of the system since in winter the pavement stays at a higher temperature and vice versa. Although, the lower thermal diffusivity layer above the embedded pipe array will improve the efficiency of the PSHSs, it must be noted that the pavement materials which surround the pipes themselves must also have a suitably high thermal effusivity (see Table 3) in order to allow rapid heat transfer from the pipe material.

Figure 10 goes here

The same findings might also have an application to pavements in cold regions – which are subjected to annual freeze-thaw cycles and deep frost penetration. From Figures 9 and 10 it can be further concluded that pavements with a lower thermal diffusivity could help to reduce the risk of damage

due to freeze-thaw cycling by achieving a more constant temperature at shallower depth (Figure 9) and also less temperature fluctuation (Figure 10).

Changing concrete composition in order to modify the thermal properties of the mix cannot be performed in isolation from an effect on the other properties of the concrete – specifically on the mechanical properties. Thus thermally desirable changes to the concrete's make-up could have a deleterious effect on the strength of the concrete mixture. However, all mixes used in PHC design #1-4 (see Figure 4) and PSHS design #1-5 (see Figure 8) meet mechanical requirements to be an airfield pavement (*6*). The same materials as introduced in this paper have also been subjected to a mechanical testing programme. When this programme is complete, the authors plan to publish the results in a future paper. At present it appears that thermal modification can be achieved and mechanically-adequate performance retained, although not always easily. It is probable that some compromise between the two goals will be necessary or the thermally-adapted materials utilized in a pavement sequence adapted to employ them successfully.

CONCLUSIONS

The study has determined the thermo-physical properties of concrete pavement materials and their effects on the performance of PHC and PSHS and other implications to help pavement design. The following conclusions can be drawn on the basis of the results and analysis proposed in this study.

1. The thermal conductivity of the concrete was directly and positively related to its degree of saturation as well as the thermal conductivity of its aggregates. However it was negatively related to the concrete porosity.
2. The thermal conductivity of concrete can be significantly increase by generating a continuous highly conductive path (e.g. addition of metallic fibres).
3. High thermal diffusivity concrete, which can be achieved by incorporating high conductive aggregate and/or addition of metallic fibres, can significantly enhance heat transfer to the embedded pipe networks.
4. By using high diffusivity concrete in hot climates warping stresses that occur due to temperature differences between the top and bottom of the slab can be reduced.
5. Low thermal diffusivity concrete, which can be achieved by using high VHC aggregates and/or low conductivity aggregates, can induce a more stable temperature at shallower depth enabling easier heat storage in the pavement.
6. By using low diffusivity concrete in cold climates the risk of damage due to freeze-thaw cycling can be minimised.

ACKNOWLEDGMENTS

The authors wish to acknowledge the financial support of this research by the Engineering and Physical Sciences Research Council (EPSRC) and East Midlands Airport.

REFERENCES

1. Carder, D.R., K. J. Barker., M. G. Hewitt., D. Ritter and A. Kiff. Performance of an interseasonal heat transfer facility for collection, storage, and re-use of solar heat from the road surface. *Transport Research Laboratory*, Published Project Report, PPR 302, 2007.
2. de Bondt, A. Generation of Energy Via Asphalt Pavement Surfaces, Prepared for Asphaltica Padova, Netherland, 2003. Also available online at: http://www.roadenergysystems.nl/pdf/Fachbeitrag%20in%20OIB%20-%20de%20Bondt%20-%20English%20version%2013-11-2006.pdf
3. Yavuzturk, C., K. Ksaibati and A. D. Chiasson. Assessment of Temperature Fluctuations in Asphalt Pavements Due to Thermal Environmental Conditions Using a Two-Dimensional, Transient Finite-Difference Approach. *Journal of Materials in Civil Engineering*, Vol 17, No. 4, 2005, pp 465–475.
4. Gui, J., P. E. Phelan., K. E. Kaloush and J. S. Golden. Impact of Pavement Thermophysical Properties on Surface Temperatures. *Journal of Materials in Civil Engineering*, Vol 19, No. 8, 2007, pp 683–690.
5. Keikha, P., M. R. Hall and A. R. Dawson. Concrete pavements as a source of heating and cooling", *Proc 11th International Symposium on Concrete Roads*, 13th – 15th October, Seville, Spain, 2010.
6. Defence Estates. *Design and Maintenance guide 20, A Guide to Airfield Pavement Design and Evaluation*, Second Edition, UK, 2006.
7. BSI, BS EN 12620:2002+A1:2008. *Aggregates for Concrete*. British Standards Institution, London, 2002.
8. BSI, BS EN 1097-6: 2000. *Tests for Mechanical and Physical Properties of Aggregates. Part 6: Determination of Particle, Density and Water Absorption*. British Standards Institution, London, 2000.
9. BSI, BS EN 12390-3:2009. *Testing hardened concrete, Part 3: Compressive strength of test specimens*, British Standard Institution, London, 2009.
10. ISO, 8301: 1996. *Thermal Insulation – Determination of Steady-State Thermal Resistance and Related Properties – Heat Flow Meter Apparatus*, International Organization for Standardization, Geneva, Switzerland, 1996.
11. Cook, D. J. and C. Uher. The Thermal Conductivity of Fibre-Reinforced Concrete. *Cement and Concrete Research*, Vol 4, 1974, pp 497–509.
12. US Department of Transportation – Federal Transport Administration, LTPP Seasonal Monitoring Programme (SMP): Pavement Performance Database (PPDB), DVD Version, Standard Data Release 23.0, USA, 2009.
13. ASHRAE, Commercial/institutional ground source heat pump engineering manual, American Society of Heating, Refrigerating and Air- Conditioning Engineers Inc. Atlanta, 1995.
14. Cote, J. and J. M. Konrad. Thermal Conductivity of Base-Course Materials, *Canadian Geotechnical Journal*, Vol. 42, No. 2, 2005, pp. 443-458.
15. Banks, D. *An Introduction to Thermogeology: Ground Source Heating and Cooling*. Blackwell Publishing Ltd. Oxford, 2008.
16. Najim, K. B. and M. R. Hall. A review of the fresh/hardened properties and applications for plain- (PRC) and self-compacting rubberised concrete (SCRC). *Construction and Building Materials*, Vol 24, No. 11, 2010, pp. 2043–2051.
17. Cverna, F. ed. *Thermal Properties of Metals.* ASM International Materials Park, Ohio, 2002.
18. Beall, C. and Jaffe, R. *Concrete and Masonry Databook*. McGraw Hill. New York,

2002.
19. Sedgwick, R. H. D. and M. A. Patrick. The Use of a Ground Solar Collector for Swimming Pool Heating. Solar World Forum, *Proceedings of ISES*, Brighton, England, 1981, pp. 632-636.

List of Figures

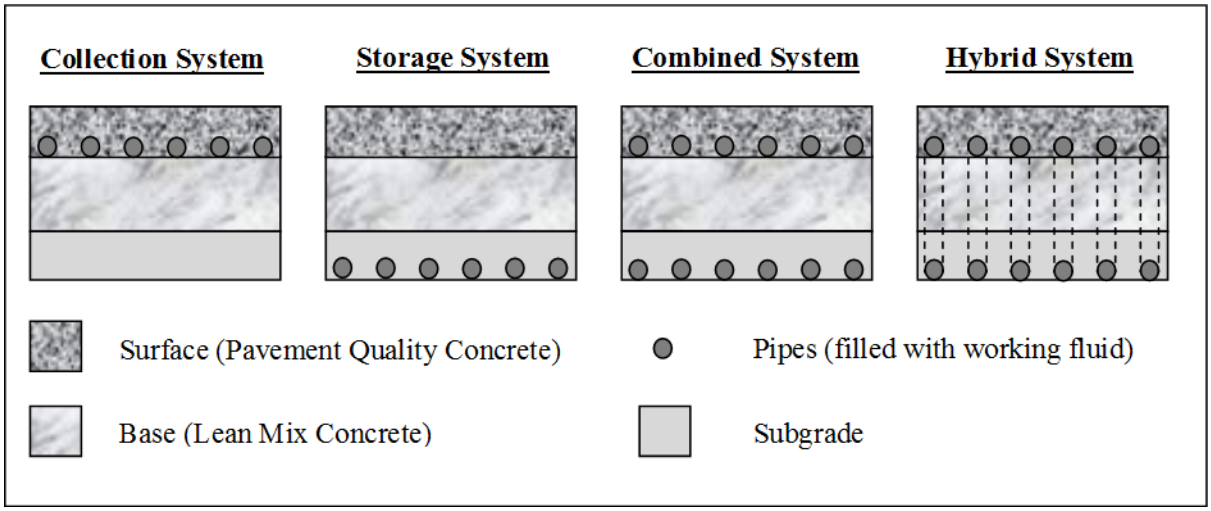

Figure 1 Applications of solar pavements

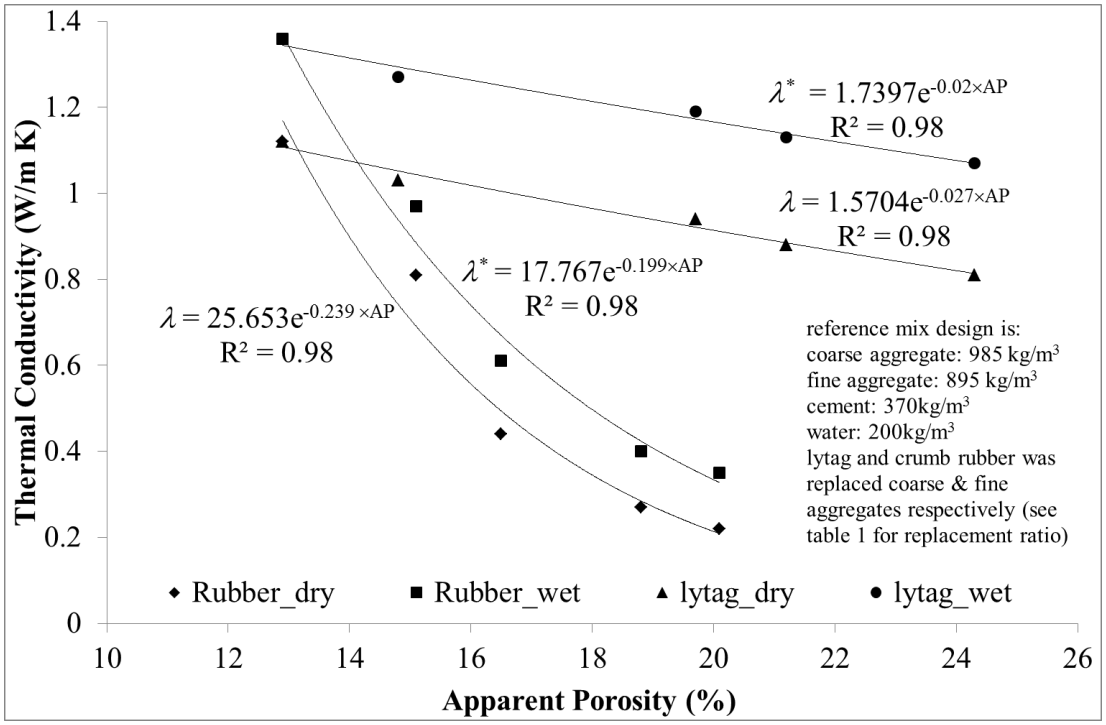

Figure 2 Relationship between Apparent Porosity of Lytag-and crumb rubber- modified concretes with wet and dry thermal conductivity

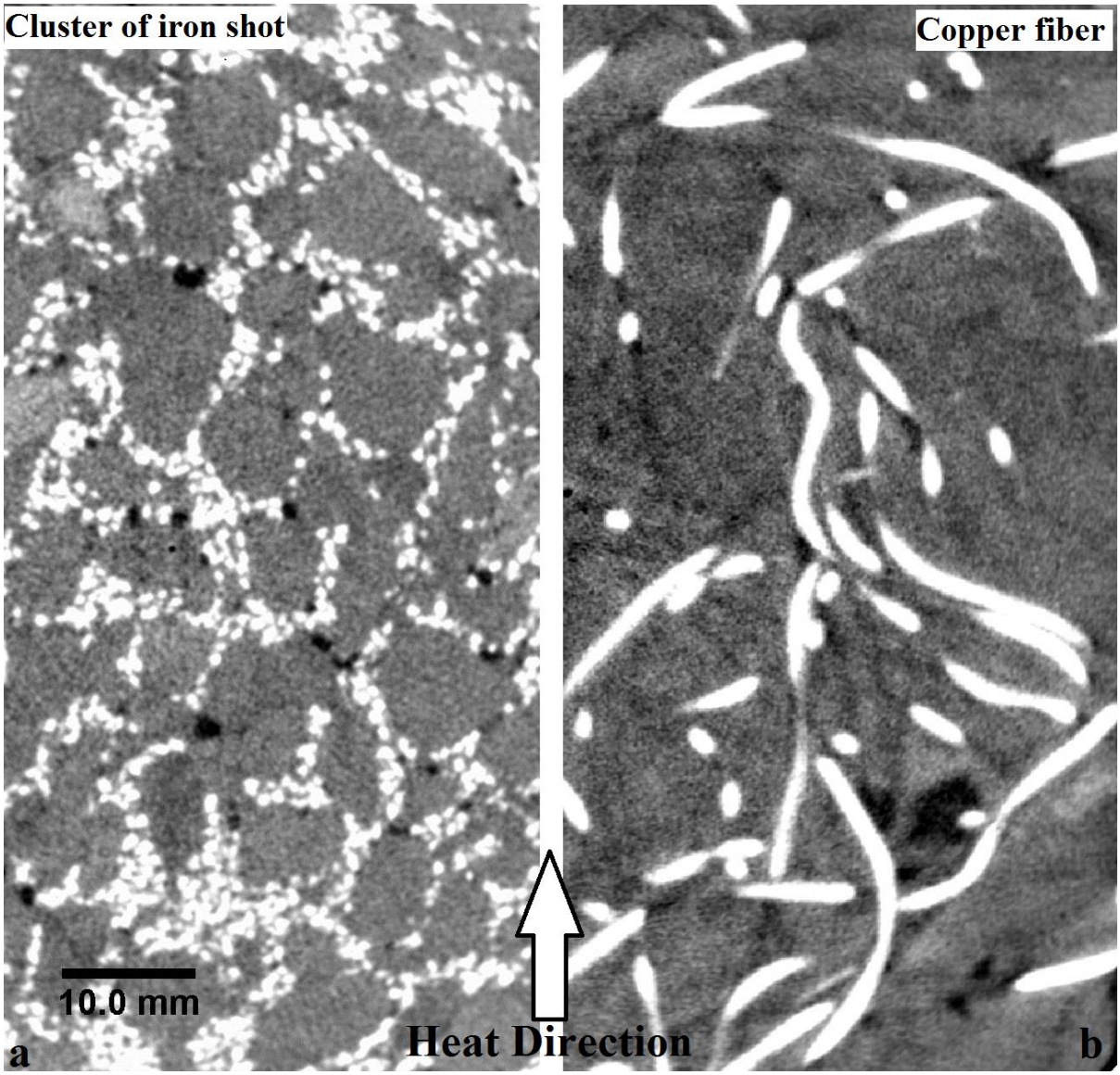

Figure 3 XRCT images of concrete containing (a) iron shot replaced NS (b) 2% (by concrete volume) copper fibre addition

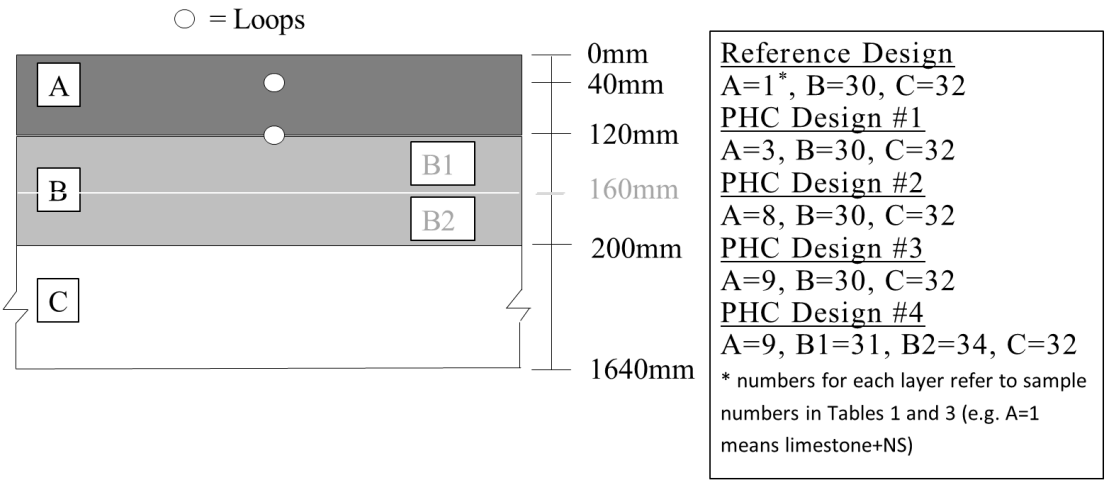

Figure 4 Cross- section of modified pavements for PHC applications

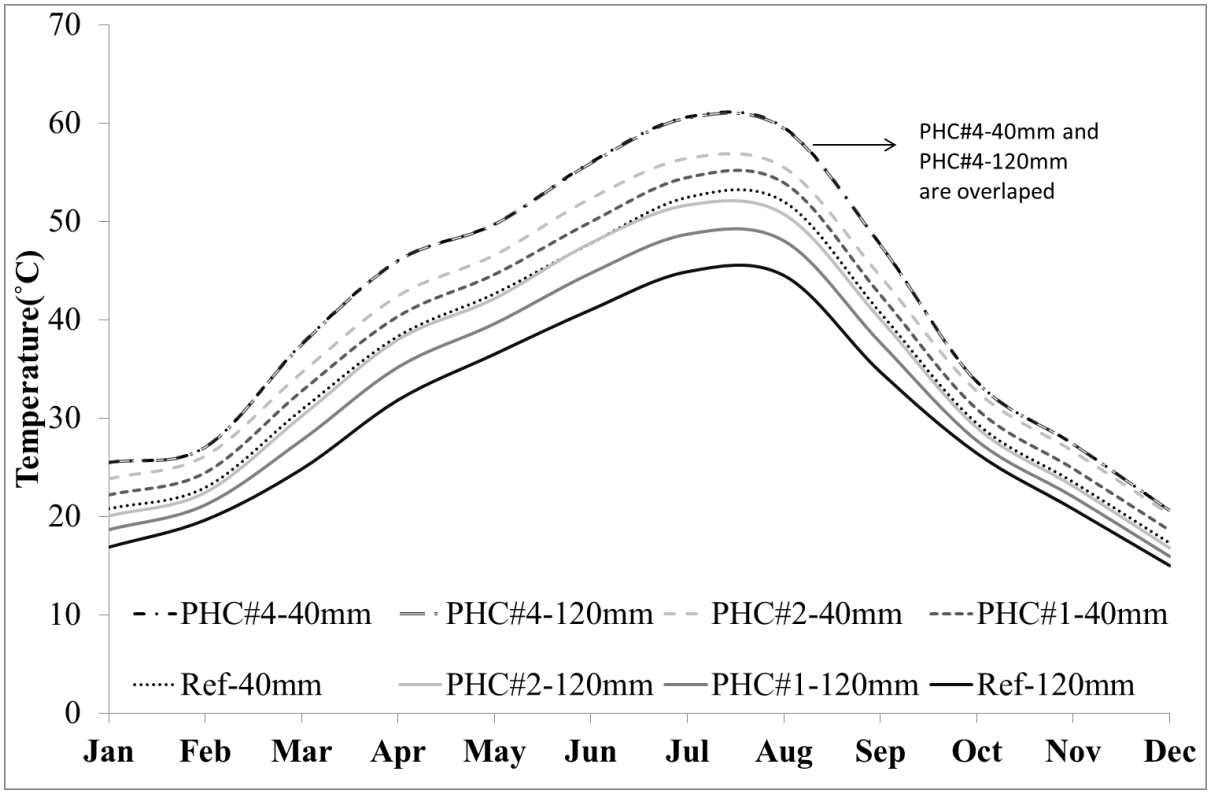

Figure 5 Mean maximum monthly temperatures at depths of 40mm and 120mm in Arizona for PHC designs

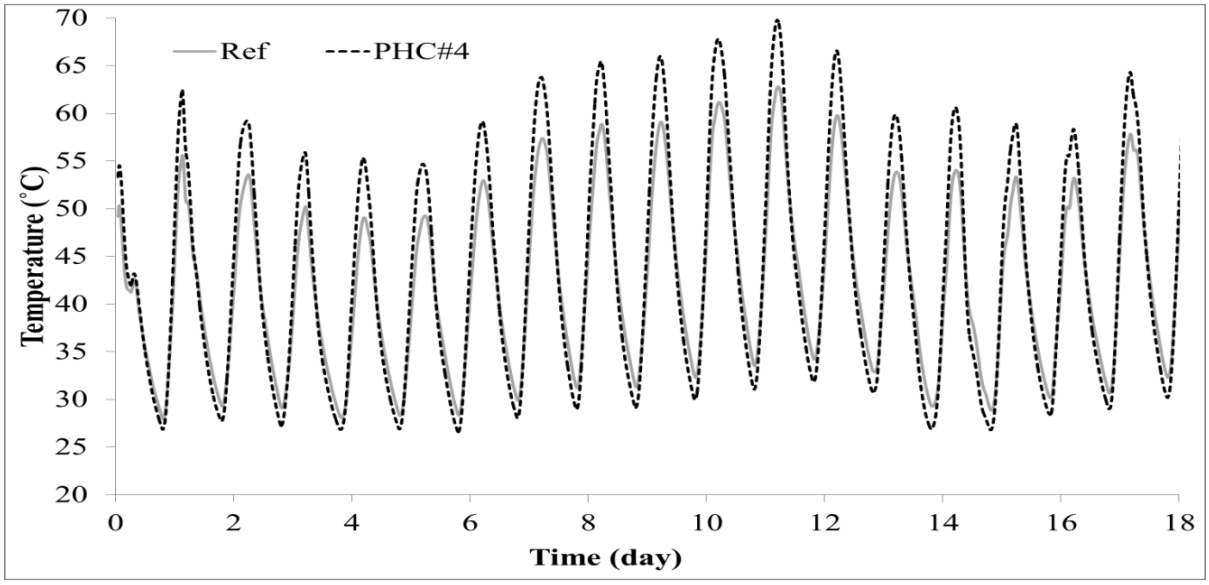

Figure 6 Comparison of the predicted temperature at 40mm depth in July for the unmodified reference pavement and PHC design #4

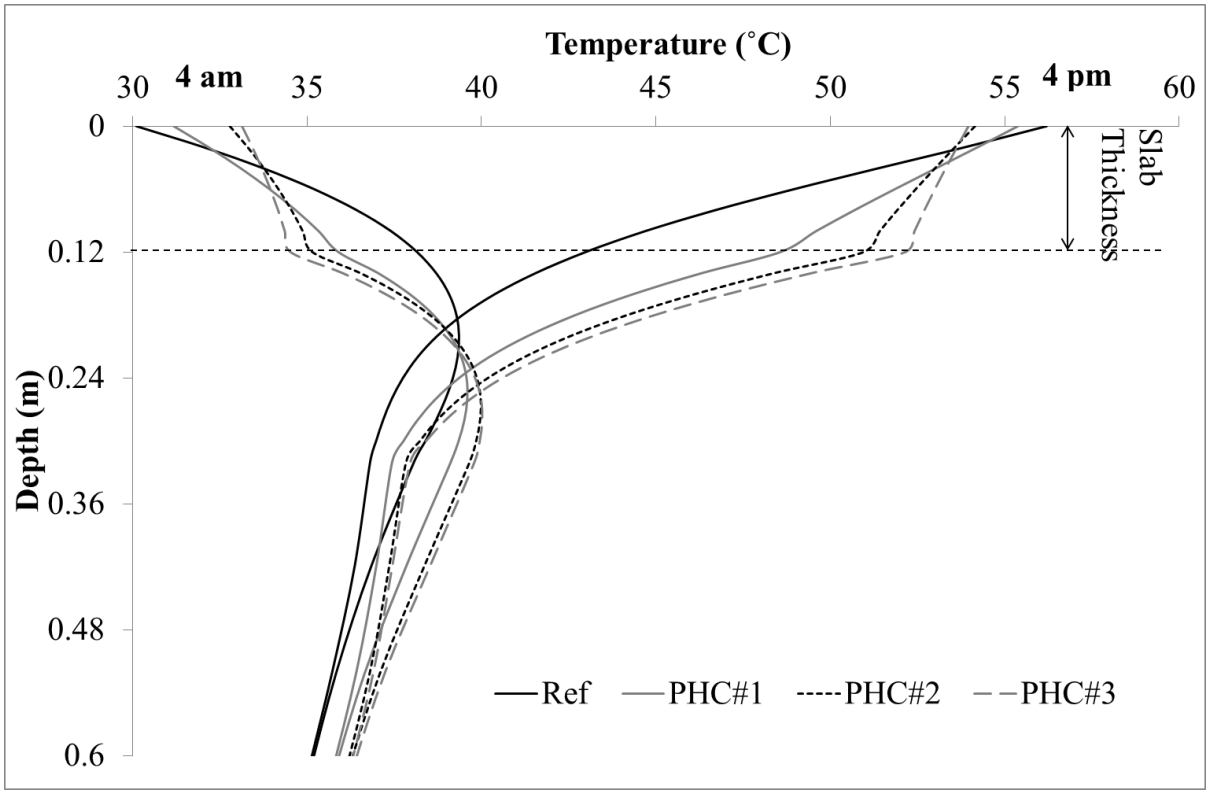

Figure 7 Comparison of the temperature distribution across 120 mm concrete slabs for the reference pavement, and PHC Designs #1, #2, and #3 at 4am and 4pm in July

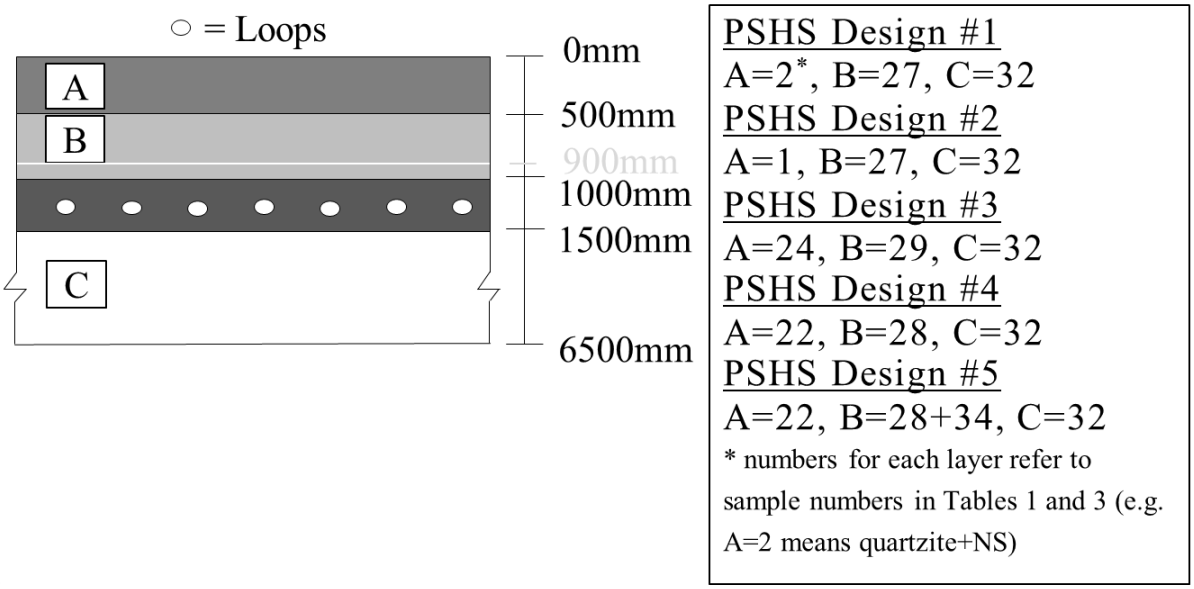

Figure 8 Cross- section of modified pavements for PSHS applications

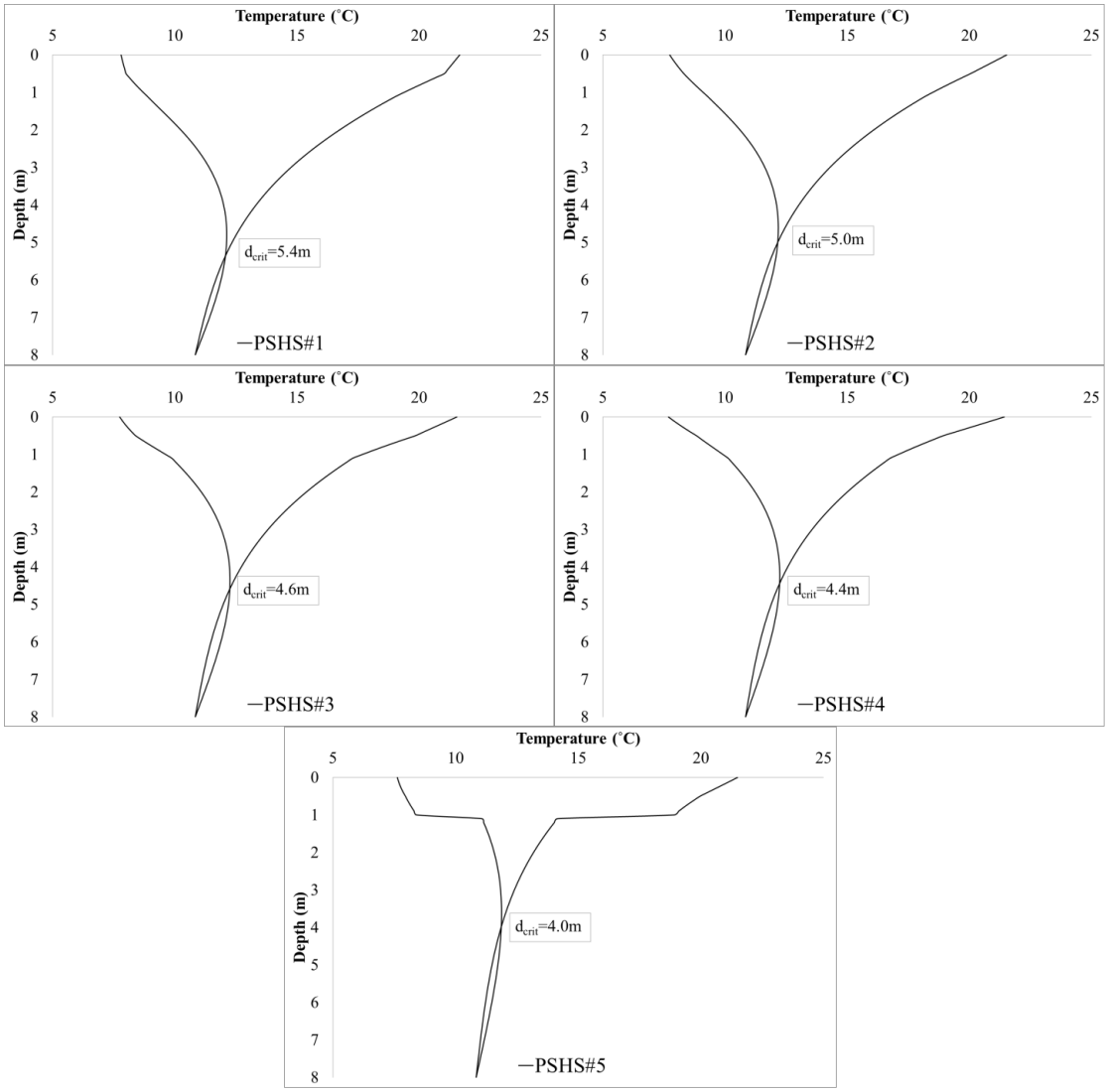

Figure 9 critical depths (d_{crit}) for different PSHS designs

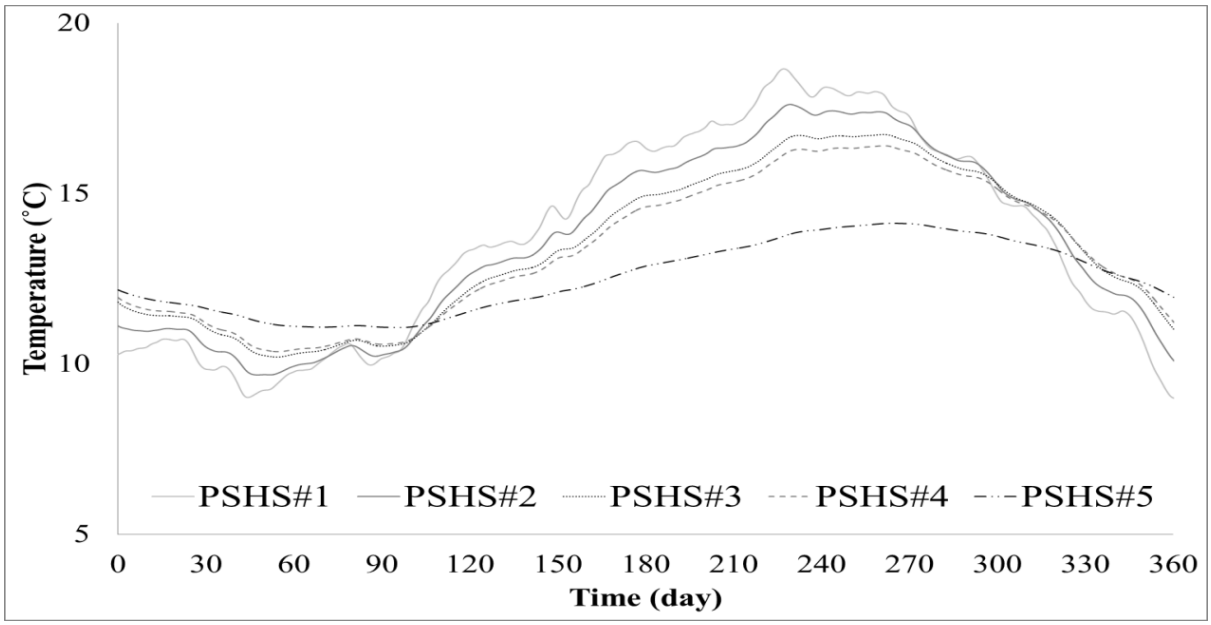

Figure 10 Temperature fluctuations at 1.5m depth for different PSHS designs

List of Tables

TABLE 1 Physical and Mechanical Properties of Modified Concrete Pavement Materials

Sample No	Concrete		ρ_d (kg/m^3)	ρ_{ssd} (kg/m^3)	f_c MPa	*AP* (%)
	Coarse Aggregate	Fine Aggregate				
1	Limestone	NS	2190	2320	52	12.9
2	quartzite	NS	2250	2387	52	13.7
3	quartzite	quartzite	2268	2343	51	7.5
4[a]	Gravel	Sand	2155			
5[a]	Gravel	Sand+0.5%CU_Fibre	2210			
6[a]	Gravel	Sand+1%CU_Fibre	2250			
7[a]	Gravel	Sand+2%CU_Fibre	2350			
8[a]	Gravel	Sand+4%CU_Fibre	2400			
9[a]	Gravel	Sand+8%CU_Fibre	2590			
10	CS	NS	2638	2755	51	11.6
11	CS	CS	2985	3105	49	11.9
12	CS	20%rubber+80%CS	2832	2956	33	12.4
13	CS	50%rubber+50%CS	2575	2708	27	13.3
14	limestone	80%NS+20%rubber[b]	2079	2231	35	15.1
15	limestone	50%NS+50%rubber	1929	2096	14	16.6
16	limestone	20%NS+80%rubber	1712	1901	8	18.8
17	limestone	rubber	1531	1730	3	20.0
18	80%limestone+20%lytag	NS	2084	2233	49	14.8
19	50%limestone+50%lytag	NS	1919	2120	46	20.1
20	20%limestone+80%lytag	NS	1809	2026	31	21.7
21	Lytag	NS	1699	1948	40	24.9
22	Lytag	Lytag	1412	1706	37	29.4
23	Lytag	CS	2238	2325	41	8.8
24	CS	Iron Shot	4258	4354	47	9.6
25	IBA	NS	2018	2118	41	9.9
26	FBA	NS	1886	2014	29	12.8
27[c]	Limestone	Limestone	2158	2278	15	12.0
28[c]	Lytag	Lytag	1568	1788	12	21.9
29[c]	CS	CS	3080	3201	14	12.1
30[d]	Crushed Aggregate		2191			
31	Loose Lytag			800		
32[e]	Heavy Soil (Clay, Compacted Sand, Loam)		2000	2100		
33[e]	Light Soil (Loose Sand, Silt)		1450	1600		
34[f]	Polystyrene		30			

ρ_d dry density
ρ_{ssd} saturated surface dry density
f_c compressive strength
AP apparent porosity
NS, Natural Sand; CS, Copper Slag; IBA, Incinerator Bottom Ash; FBA, Furnace Bottom Ash.
[a] (reference *11*) [b] (crumb rubber particle size is 2-4mm), [c] (Values are for LMC),[d] (reference *12*),[e] (reference *13*),[f] (reference 1)

TABLE 2 Mean Value of Specific Heat Capacity of Concrete Components (J/kg K)

Temperature (˚C)	HCP	CS	Lytag	NS	Quartzite	Limestone	IBA	FBA	Iron Shot	Rubber
-13	807	522	546	495	450	793	599	571	401	960
0	1021	670	712	637	629	838	748	678	552	1292
7	1094	679	741	655	642	859	787	703	562	1326
17	1241	691	767	679	659	878	850	732	575	1369
27	1458	701	778	698	675	892	917	751	586	1406
37	1714	712	787	711	693	904	956	768	589	1444
47	1978	723	799	721	709	917	978	782	609	1485
57	2300	734	812	734	724	931	984	793	618	1523

HCP, Hardened Cement Paste; CS, Copper Slag; NS, Natural Sand; IBA, Incinerator Bottom Ash; FBA, Furnace Bottom Ash

TABLE 3 Thermal Properties of Modified Concrete Pavements

Sample No	Concrete		λ (W/m K)[a]	λ^* (W/m K)	C_p (J/ kg K)[b]	C_p^* (J/kg K)	α ($\times 10^{-7}$) (m^2/s)	α^* ($\times 10^{-7}$) (m^2/s)	β ($J/s^{0.5}m^2K$)	β^* ($J/s^{0.5}m^2K$)
	Coarse Aggregate	**Fine Aggregate**								
1	Limestone	NS	1.12	1.36	953	1114	5.37	5.26	1529	1875
2	quartzite	NS	2.64	2.81	860	1031	13.64	11.42	2260	2630
3	quartzite	quartzite	2.98	3.08	852	948	15.42	13.87	2400	2616
4[c]	Gravel	Sand	1.530		1080		6.57		1887	
5[c]	Gravel	Sand+0.5%CU-Fibre	2.096		1070		8.86		2226	
6[c]	Gravel	Sand+1%CU-Fibre	2.677		1060		11.22		2527	
7[c]	Gravel	Sand+2%CU-Fibre	3.251		1040		13.30		2819	
8[c]	Gravel	Sand+4%CU-Fibre	5.980		995		25.04		3779	
9[c]	Gravel	Sand+8%CU-Fibre	10.71		920		44.95		5052	
10	CS	NS	1.18	1.29	854	986	5.23	4.75	1630	1872
11	CS	CS	0.81	0.94	837	958	3.24	3.16	1423	1672
12	CS	20%rubber+80%CS	0.64	0.75	863	995	2.62	2.55	1251	1485
13	CS	50%rubber+50%CS	0.57	0.71	908	1060	2.44	2.47	1154	1428
14	limestone	80%NS+20%rubber	0.81	0.97	987	1180	3.95	3.68	1289	1598
15	limestone	50%NS+50%rubber	0.44	0.61	1043	1263	2.19	2.30	940	1271
16	limestone	20%NS+80%rubber	0.27	0.40	1110	1369	1.42	1.54	716	1020
17	limestone	rubber	0.22	0.36	1160	1444	1.24	1.44	625	948
18	80%limestone+ 20%lytag	NS	1.03	1.27	950	1140	5.20	4.99	1428	1798
19	50%limestone+ 50%lytag	NS	0.94	1.19	945	1207	5.18	4.65	1306	1745
20	20%limestone+ 80%lytag	NS	0.88	1.13	939	1236	5.18	4.51	1170	1682
21	Lytag	NS	0.81	1.07	935	1285	5.10	4.27	1134	1637
22	Lytag	Lytag	0.46	0.71	1009	1481	3.23	2.81	809	1339
23	Lytag	CS	0.67	0.78	900	1017	3.33	3.30	1162	1358
24	CS	Iron Shot	1.21	1.31	729	800	3.90	3.76	1938	2136
25	IBA	NS	0.86	1.18	968	1108	4.20	5.03	1328	1664
26	FBA	NS	1.05	1.14	942	1150	5.53	4.92	1411	1625
27[d]	Limestone	Limestone	0.92	1.16	983	1227	4.34	4.15	1397	1800
28[d]	Lytag	Lytag	0.56	0.88	953	1574	3.75	3.13	915	1574
29[d]	CS	CS	0.84	0.99	761	880	3.58	3.51	1403	1670
30[e]	Crushed Aggregate		0.7	1.3	892		3.58		1170	
31	Loose Lytag		0.20	0.34	778		3.21		353	
32[f]	Heavy Soil (Clay, Compacted Sand, Loam)		0.86	1.30	840	960	5.12	6.45	1202	1619
33[f]	Light Soil (Loose Sand, Silt)		0.34	0.86	840	1040	2.79	5.17	643	1196
34[g]	Polystyrene		0.034		1130					

λ oven-dry thermal conductivity, λ^* water-immersed thermal conductivity
c_p dry- state specific heat capacity, c_{p*} wet-state specific heat capacity
α dry-state thermal diffusivity, α^* wet-state thermal diffusivity
β dry-state thermal effusivity, β^* wet-state thermal effusivity

[a] (Values for λ were determined under steady state conditions at 1% stability), [b] (Values for c_p and c_p^* were calculated at 27˚C, [c] (reference *11*), [d] (Values are for LMC), [e] (reference *15*),[f] (reference *13*),[g] (reference *1*)